JACS
JOURNAL OF THE AMERICAN CHEMICAL SOCIETY
Article
Cite This: J. Am. Chem. Soc. 2018, 140, 10504−10513
pubs.acs.org/JACS

Targeted Ligand-Exchange Chemistry on Cesium Lead Halide Perovskite Quantum Dots for High-Efficiency Photovoltaics

Lance M. Wheeler,*[,†] Erin M. Sanehira,[†,‡] Ashley R. Marshall,[†,∥] Philip Schulz,[†,⊥] Mokshin Suri,[§] Nicholas C. Anderson,[†] Jeffrey A. Christians,[†] Dennis Nordlund,[#] Dimosthenis Sokaras,[#] Thomas Kroll,[#] Steven P. Harvey,[†] Joseph J. Berry,[†] Lih Y. Lin,[‡] and Joseph M. Luther*[,†]

[†]National Renewable Energy Laboratory, Golden, Colorado 80401, United States
[‡]Department of Electrical Engineering, University of Washington, Seattle, Washington 98195, United States
[§]McKetta Department of Chemical Engineering and Texas Materials Institute, The University of Texas at Austin, Austin, Texas 78712-1062, United States
[∥]Department of Chemistry and Biochemistry, University of Colorado, Boulder, Colorado 80309, United States
[⊥]CNRS, Institut Photovoltaïque d'Île de France (IPVF), UMR 9006, 91120 Palaiseau, France
[#]Stanford Synchrotron Radiation Lightsource, SLAC National Accelerator Laboratory, Menlo Park, California 94025, United States

Supporting Information

ABSTRACT: The ability to manipulate quantum dot (QD) surfaces is foundational to their technological deployment. Surface manipulation of metal halide perovskite (MHP) QDs has proven particularly challenging in comparison to that of more established inorganic materials due to dynamic surface species and low material formation energy; most conventional methods of chemical manipulation targeted at the MHP QD surface will result in transformation or dissolution of the MHP crystal. In previous work, we have demonstrated record-efficiency QD solar cells (QDSCs) based on ligand-exchange procedures that electronically couple MHP QDs yet maintain their nanocrystalline size, which stabilizes the corner-sharing structure of the constituent PbI_6^{4-} octahedra with optoelectronic properties optimal for solar energy conversion. In this work, we employ a variety of spectroscopic techniques to develop a molecular-level understanding of the MHP QD surface chemistry in this system. We individually target both the anionic (oleate) and cationic (oleylammonium) ligands. We find that atmospheric moisture aids the process by hydrolysis of methyl acetate to generate acetic acid and methanol. Acetic acid then replaces native oleate ligands to yield QD surface-bound acetate and free oleic acid. The native oleylammonium ligands remain throughout this film deposition process and are exchanged during a final treatment step employing smaller cations—namely, formamidinium. This final treatment has a narrow processing window; initial treatment at this stage leads to a more strongly coupled QD regime followed by transformation into a bulk MHP film after longer treatment. These insights provide chemical understanding to the deposition of high-quality, electronically coupled MHP QD films that maintain both quantum confinement and their crystalline phase and attain high photovoltaic performance.

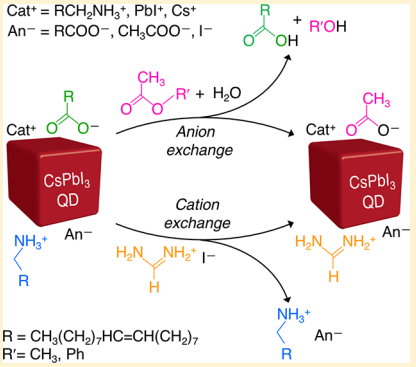

INTRODUCTION

Metal halide perovskites (MHPs) have quickly risen to prominence as materials with a rich, tunable chemistry that have yielded unprecedented performance in optoelectronic technologies for photon emission and solar cell applications.[1] Colloidal synthesis of quantum-confined MHP structures offers yet another level of tunability and promise for optoelectronics.[2] MHP quantum dots (QDs) show size- and composition-dependent optical properties[2] with a bandgap that can be tuned throughout the ultraviolet[3] to infrared.[4]

Control of composition and size is afforded by hot injection synthesis.[2] During the injection reaction, cations (Pb^{2+}, Cs^+, and $RCH_2NH_3^+$, where R = oleyl = $CH_3(CH_2)_7HC{=}CH(CH_2)_7$) and anions ($I^-$, $RCOO^-$) arrange to form stoichiometric crystalline $CsPbI_3$ cores. The resulting surface is terminated with ligands that cooperatively bind to the QD surface as highly dynamic[5] ion pairs that are dramatically impacted by acid−base chemistry of the solution.[7,8] The highly ionic nature of the surface species makes QD surface manipulation a new frontier in colloidal QD chemistry compared to highly covalent systems like Si[6,7] or Ge[8,9] with X-type ligands or the more heavily explored II−VI[10−14] or IV−VI[15−17] QDs that commonly bind ligands as Z-type Lewis acids or L-type Lewis bases. To date, there are a number of reports on the surface modification of $CsPbX_3$, where X = Br or I.[18−21] Native ligands have been exchanged for bifunctional molecules,[19,20] and ion-pair ligand exchange has yielded high-performance

Received: May 12, 2018
Published: July 25, 2018

DOI: 10.1021/jacs.8b04984
J. Am. Chem. Soc. 2018, 140, 10504−10513

Scheme 1. (a) Hydrolysis of an Ester To Yield a Carboxylic Acid and an Alcohol; (b) Anionic Carboxylate Ligand-Exchange Reaction Observed in $CsPbI_3$ Thin Films and Solutions; (c) Cationic Ligand Exchange Observed in $CsPbI_3$ Thin Films

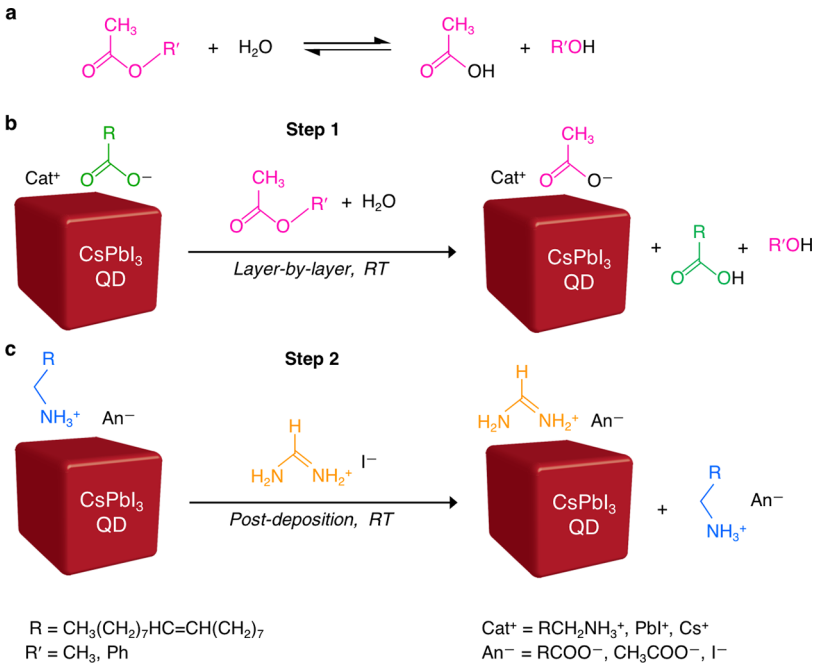

LEDs[22] as well as enhanced ambient stability.[23] Most notably, surface manipulation has led to a number of reports of near-unity photoluminescence quantum yield (PLQY) in MHP QDs without a need for complex passivating shells typically required for high PLQY in other QD emitter materials.[21−23]

In contrast to emitter applications, photovoltaics (PVs) require strong coupling between QDs, which is achieved by purifying the QDs to remove residual precursors and reaction solvent followed by replacing the native ligands with more compact surface species for functional electronically coupled films.[9] For MHP QDs, problems arise during purification. In typical QD systems (groups II−VI, IV−VI), polar solvents are added to precipitate colloidal QDs, but many polar solvents dissolve components of the MHP crystal or QD surface species. Methyl acetate (MeOAc) strikes a desirable balance between low surface ion solubility and the polarity necessary for QD precipitation.[24]

In addition to the unique purification challenges in MHP QDs, improved inter-QD coupling must be accomplished without destructively modifying the structure of the QDs. Slightly different from the history on PbS and PbSe[25] QD solar cells (QDSCs),[25−28] a two-step solid-state QD ligand-exchange procedure is used to form electrically coupled $CsPbI_3$ QD films and yields record-efficiency QDSCs with low voltage losses as well as LEDs.[24,29] Here we present a molecular picture of the QD surface during each of these steps through data obtained by a variety of analytical techniques. Oleate ligands are targeted in the first step by exchange with acetate, which is formed *in situ* via hydrolysis of MeOAc with adventitious water. The final treatment using formamidinium iodide (FAI) in ethyl acetate (EtOAc) yields solvated formamidinium (FA^+) cations which specifically target oleylammonium cations. Ligand exchange is critical to the formation of high-efficiency QDSCs, making a detailed understanding of the surface chemistry throughout this process of utmost importance.

RESULTS AND DISCUSSION

We performed experiments to understand each step in the QD film deposition process (Scheme 1). The first ligand exchange targets native oleate ligands. We find oleate removal first occurs during the washing step via hydrolysis of the precipitating antisolvent, MeOAc, to yield acetic acid and methanol (Scheme 1a). Acetic acid molecules then protonate QD-bound oleate ligands to yield QD-bound acetate and free oleic acid and methanol (Scheme 1b).

The chemistry of the $CsPbI_3$ QD surface following interaction with MeOAc was determined by a combination of Fourier transform infrared (FTIR) and nuclear magnetic resonance (NMR) spectroscopies. Figure 1a shows a FTIR spectrum of the solid $CsPbI_3$ QD pellet that results from centrifugation of the QD solution (green spectrum). The QDs have not been exposed to MeOAc in this case and largely resemble spectra of $CsPbBr_3$ observed in previous work.[30] The FTIR spectrum of the centrifuged QDs is dominated by vibrational modes of bound and unbound ligand molecules. Oleylammonium is distinguished from the excess oleylamine in solution (OAm, black spectrum in Figure 1a). Though both molecules have resonances due to the oleyl group ($\nu(C-H_x)$ = 2780−3000 cm^{-1}, $\nu(C{=}C-H)$ = 3005 cm^{-1}, and $\nu(C-H_2)$ = 1466 cm^{-1}),[14,15] we attribute the broad resonance centered at 3138 cm^{-1} to stretching vibrations of ammonium groups, $\nu(N-H_3^+)$. Oleic acid (blue spectrum, Figure 1a) is also distinguishable from oleate. Oleic acid and oleate share oleyl resonances with oleylamine/oleylammonium, but oleic acid has a characteristic carboxylic acid resonances, $\nu(C{=}O)$ = 1708 cm^{-1} and $\nu(O-H)$ = 2500−3250 cm^{-1}, and oleate has resonances due to the bound carboxylate group, where symmetric ($\nu_s(COO^-)$ = 1409 cm^{-1}) and asymmetric ($\nu_{as}(COO^-)$ = 1530 cm^{-1}) stretching modes are observed.[31,32]

A relative intensity increase of the carboxylate resonances compared to the oleyl resonances is observed when the QDs are precipitated from solution with the addition of MeOAc (yellow spectrum, Figure 1a). This suggests a larger concentration of carboxylate species compared to oleyl species but does not necessarily imply acetate attachment to the QD surface. The disappearance of $\nu(C{=}O)$ compared to the

DOI: 10.1021/jacs.8b04984
J. Am. Chem. Soc. 2018, 140, 10504−10513

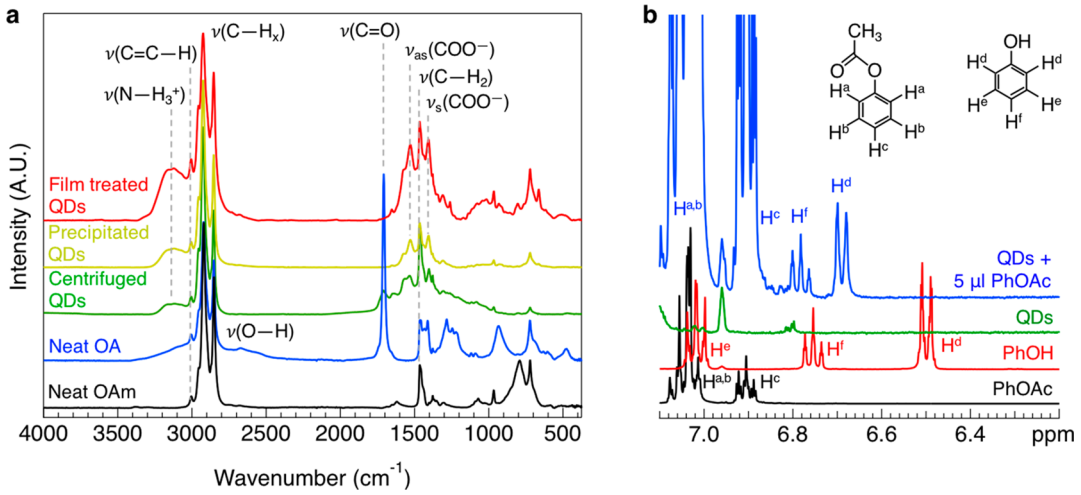

Figure 1. (a) FTIR spectra of neat OAm (black) and OA (blue) and $CsPbI_3$ QD films that were purified by centrifuging the QDs from the reaction solution (green), precipitating them with MeOAc from the reaction solution (amber), and by treating the precipitated QD film with MeOAc after deposition (red), similar to the first step in $CsPbI_3$ QD solar cell fabrication. Spectra are normalized to the most intense peak ($\nu(C-H_x)$) and offset for clarity. (b) ^1H NMR spectra of PhOAc (black), PhOH (red), solution of QDs after synthesis (green), and the same QD solution after the addition of 5 μL of PhOAc (blue). NMR spectra are taken in benzene-d_6 and offset for clarity.

centrifuged QDs suggests the intensity changes may be simply due to removal of unbound oleic acid. However, a solid-state treatment of the QDs with MeOAc (red spectrum, Figure 1a) results in additional increase in relative intensity of the carboxylate peaks to the oleyl peaks, which again suggests acetate exchange for oleate.

We employ ^1H NMR to verify the relative increase in FTIR signal intensity of the carboxylate peaks following MeOAc treatment is due to exchange of oleate for acetate. In this experiment, we use phenyl acetate (PhOAc) as the precipitating antisolvent instead of MeOAc to leverage spectrally isolated aromatic protons that are not convolved with proton resonances of aliphatic ligands at lower frequencies (Figure 1b). PhOAc precipitates $CsPbI_3$ QDs in a similar manner as MeOAc. A baseline spectrum was taken on QDs that were centrifuged and solvated in benzene-d_6 (green, Figure 1b) to show the aromatic protons of PhOAc are spectrally distinct to species left over from QD synthesis (excess ligand, reaction solvent, etc.). After the addition of 5 μL of PhOAc to the solution of QDs, the QDs precipitate, and the resultant supernatant is characterized (blue spectrum, Figure 1b). Aromatic protons due to PhOAc (H^a, H^b, and H^c) are observed in the supernatant spectrum at chemical shift (δ) = 6.9 and 7.0 ppm. The peaks in the precipitated QD spectrum (blue) are corroborated with a neat solution of PhOAc in benzene-d_6 (black spectrum, Figure 1b). Additional resonances are also observed in the precipitated QD spectrum due to the hydrolysis of PhOAc to form acetic acid and phenol (PhOH) (Scheme 1a where R′ is a phenyl group, Ph). The doublet of the ortho proton (H^d, δ = 6.7 ppm) and triplet of the para proton (H^f, δ = 6.8 ppm) are spectrally isolated from the other resonances to clearly show the formation of PhOH—a product of PhOAc hydrolysis. The sharp resonances of the PhOH protons indicate the molecule does not coordinate to the QD surface. In this case, acetate binds to the QD and oleic acid leaves the QD surface, the same as the MeOAc case.

The relative FTIR intensity of $\nu(N-H_3^+)$ also increases for both samples treated with MeOAc (Figure 1a), indicating the oleylammonium ligands are not removed during the process. Other cations (Cat^+ = PbI^+, Cs^+, etc.) that may charge-balance oleate likely behave similarly (Scheme 1b) but have no clear FTIR fingerprint to verify that they remain after carboxylate exchange. Thus, X-ray photoelectron spectroscopy (XPS) was used to determine elemental composition of the $CsPbI_3$ QD film surfaces before and after MeOAc treatment (Table 1, Figure S1). As suggested by the FTIR data, the N:Pb ratio measured by XPS does not change after the MeOAc treatment. Additionally, ratios of Cs:Pb and I:Pb remain the same within the uncertainty of the measurement (~1%). No change in the stoichiometry of the $CsPbI_3$ compound indicates a selective exchange of oleate for acetate without side reactions. Interestingly, the low I:Pb ratio is less than the nominal value of 3 and less than 3.2 or 3.5, which has been reported for Br:Pb in the $CsPbBr_3$ QD analog.[18,19] However, this finding is in agreement with other reports of XPS measurements taken on slightly halide deficient lead iodide-based perovskite thin films.[23] We reconcile the iodide deficiency with preferential binding affinity of carboxylate to open lead sites on the QD surface. Similarly, the Cs:Pb ratio less than the nominal value of 1 indicates oleylammonium occupies A-sites at the crystal interface.

Table 1. Elemental Composition of $CsPbI_3$ Thin Films before and after MeOAc Treatment As Measured by XPS

QD treatment	Cs:Pb	N:Pb	I:Pb	O:Pb	C:Pb
As-Cast	0.91	0.16	2.76	0.22	5.01
MeOAc	0.93	0.15	2.79	0.12	3.69

In contrast to the oleylammonium identification via the N 1s signal, the attribution of both, the C 1s and O 1s, core level signals remains somewhat ambiguous. The dominant contribution to the C 1s core level originates from adventitious carbon species, which are physisorbed on top of the QD thin-film surface. The MeOAc treatment removes a significant amount of these species and reduces the relative amount of oxygen. Because the C 1s XPS peak does not have a shoulder at 288.5 eV, we conclude the oxygen removed is not from oleic acid or oleate but unknown contaminant species with a C−O−C coordination that is expected at 286 eV (Figure S1). Loss of these carbonaceous species is further corroborated by ultraviolet

DOI: 10.1021/jacs.8b04984
J. Am. Chem. Soc. 2018, 140, 10504−10513

photoemission spectroscopy (UPS) measurements of the valence band. While the probing depth for the XPS measurements is on the order of 5 nm for the kinetic energies of electrons investigated here, the UPS technique is sensitive only to the topmost layers with a probing depth of <2 nm. As a result, the valence band spectrum of the as-cast films is dominated by sp^3 hybridized carbon moieties, whereas clear peaks of the Cs component in the QD appear for the MeOAc-treated QD film (Figure S2). Finally, additional X-ray absorption spectroscopy measurements at the N K-edge and O K-edge further confirm a loss of carbonaceous species and no variation in the amount of oleylammonium (Figure S3).

Adventitious water is known to be responsible for a number of solution-phase reactions during the processing of bulk MHP films.[33,34] Here we have shown that esters hydrolyze in the presence of adventitious water, but the mechanism is still undetermined. It may occur as a stepwise reaction, where hydrolysis occurs in solution to yield free acetic acid and alcohol (Scheme 1) before the acetic acid reaches the QD-bound oleate for the exchange reaction. Alternatively, it may be a reaction in which the QD surface must be present. No PhOH formation was observed in the ^{1}H NMR spectrum when the phenyl acetate was added to the same benzene-d_6 without the presence of $CsPbI_3$ QD surfaces.

We demonstrate the critical role of the QD surface in the hydrolysis reaction by performing ligand exchange on $CsPbI_3$ QD films in a humidity-controlled glovebox at constant temperature and fabricating QDSCs. $CsPbI_3$ QD films are deposited by spin-coating octane solutions of MeOAc-purified MHP QDs. After spin-coating a layer of QDs, the film undergoes ligand exchange by immersion as-cast in a saturated solution of $Pb(NO_3)_2$ in MeOAc followed by washing in neat MeOAc. Thicker QD films are obtained by repeating these steps (typically four layers). The relative humidity (% RH) of the glovebox atmosphere during this process is varied between <3% RH and ≥40% RH. Figure 2 shows the performance of devices as a function of the deposition humidity. From the photograph in Figure S4, the QD films exhibit uneven coverage when fabricated at <3% RH. This uneven coverage is caused by the QD film delamination during ligand exchange with the MeOAc-based solution. In effect, the native ligand shell remains too intact, resulting in solvation of portions of the underlying QD film during the deposition of subsequent QD layers (i.e., the second QD layer deposition solvates the first layer).

QD films exhibit a yellow color when the deposition procedure is performed at >30%RH. This yellowed color is indicative of formation of the orthorhombic δ-$CsPbI_3$ crystalline phase which contains edge-sharing PbI_6^{4-} octahedra instead of the corner-sharing octahedra that characterize the black phases of $CsPbI_3$. We postulate that high relative humidity yields excessive ester hydrolysis and ligand exchange which will destabilize the surface and cause the $CsPbI_3$ QDs to coalesce, leading to phase transformation into the δ-$CsPbI_3$ orthorhombic phase. In contrast to these two extrema, ligand exchanges performed between 11% and 24% RH produced films that are dark brown and highly absorbing (Figure S4).

Visual observation of smooth, black film formation correlates to enhanced PV performance in the resulting QDSC. Figure 2a shows reverse current density−voltage scans of QDSCs fabricated in varied humidity levels. The trend of device performance vs RH is also consistent across all device performance parameters as seen in Figure 2b−e. Because the RH is

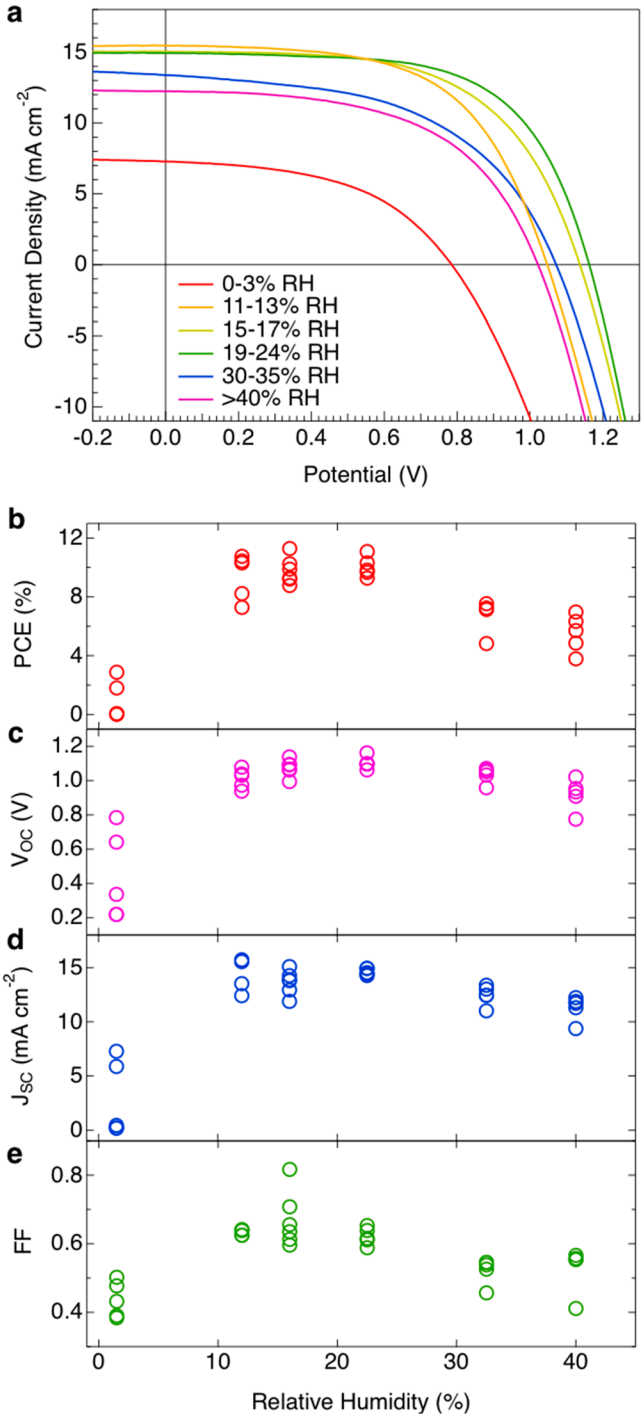

Figure 2. (a) Current density−voltage curves of $CsPbI_3$ QD-based PV devices fabricated in a climate-controlled glovebox at six different humidity levels ranging from 3 to 40% RH. (b) PCE, (c) V_{OC}, (d) J_{SC}, and (e) FF plots for five devices fabricated at each humidity.

impacting the physical ability to form the QD film (as ligand removal causes the QDs to move into closer proximity, improving electrical contact), it impacts short-circuit current density (J_{SC}), open-circuit voltage (V_{OC}), and fill factor (FF) equally. By tuning the RH to provide the ideal amount of water during the ligand-exchange procedure, we produced devices with PCE values of ∼12% and V_{OC} values of 1.2 V.

The QDSC device data suggest that atmospheric water, not necessarily water contained in the MeOAc solution, is a critical

DOI: 10.1021/jacs.8b04984
J. Am. Chem. Soc. 2018, 140, 10504−10513

variable. In this scenario, water vapor is adsorbed from the vapor phase onto the QD surface in close proximity to oleate ligands, and the hydrolysis reaction proceeds when MeOAc is accessible upon immersing the film. We fabricated devices in a ~0% RH glovebox environment with water and acetic acid controllably added to the MeOAc solution to demonstrate the role of gas-phase water adsorption. If we assume the humid glovebox environment reaches equilibrium with the initially dry MeOAc, then the concentration of water in MeOAc will be ~50 mM at 23% RH according to experimental liquid–vapor equilibrium data (Henry's law constant).[35] QDSC devices fabricated by dipping QD films in ~50 mM acetic acid solution in MeOAc yielded poorer performance compared to devices fabricated at 23% RH with PCE = 2.40 ± 0.77, FF = 0.37 ± 0.04, J_{SC} = 8.43 ± 1.45 mA cm^{-2}, and V_{OC} = 0.72 ± 0.20 V (Figure S5, statistics include 12 working pixels).

The addition of water to the MeOAc solution was also explored. A 0.8 M solution of water in addition to the ~50 mM acetic acid in MeOAc resulted in poorer and inconsistent results compared to humid atmosphere experiments with PCE = 3.87 ± 2.50, FF = 0.41 ± 0.10, J_{SC} = 10.8 ± 2.41 mA cm^{-2}, and V_{OC} = 0.77 ± 0.28 V (Figure S5, statistics include 12 working pixels). Though a PCE as high as 8.1% was achieved with a 0.8 M water in MeOAc solution, the process also yielded significantly more variation in performance, which speaks to the delicate balance between treating the surface, disrupting film morphology, and chemically modifying the bulk QD crystal (dissolution or ripening). Gas-phase adsorption of water targets QD surface sites without changing the properties of the bulk solution the film is immersed in. Though alternative processes may be optimized to achieve high PV performance, atmospheric humidity gave the most reliable, targeted strategy for ligand exchange.

Comparing vapor to solution-phase water demonstrates the sensitivity of experimental conditions needed for fabrication of efficient QDSCs. The relative humidity experimental results are important to enable repeatability of QDSC fabrication from lab to lab in different parts of the world and in the interpretation of other recent works that use ester treatments to impart functionality in $CsPbX_3$-based solar cells[31,32] and light-emitting devices.[36−38]

It is worth noting a saturated solution of $Pb(NO_3)_2$ in methyl acetate was employed during the film deposition process in past work,[12,13] and its role is briefly investigated here. We find no indication that nitrate molecules are incorporated into the QD film. There are no ν(N−O) vibrations in the FTIR spectrum after treatment (Figure S6), and no additional peaks were observed in the XPS measurements in the respective binding energy region (>405 eV) of nitrate species in the N 1s core-level spectra of the treated QD surfaces (Figure S1). We hypothesize that lead nitrate influences the amount of water able to interact with the QD surface but does not directly interact with the QD surface.

Whereas ester treatment of MHP QD films targets the anionic oleate ligand, exposure to FAI targets the oleylammonium ligands to produce highly coupled, defect-free arrays of QDs. We showed previously that treatment of MHP QD films with AX salt solutions, where A is a 1+ cation that fits in the MHP lattice and X is a halide, results in record-efficiency QDSCs.[29] Here we uncover a molecular picture of the process during FAI treatment (Scheme 1c) and find FAI exchanges with salt pairs on the QD surface, in contrast to the previous MeOAc treatment, which selectively exchanges with anionic ligands.

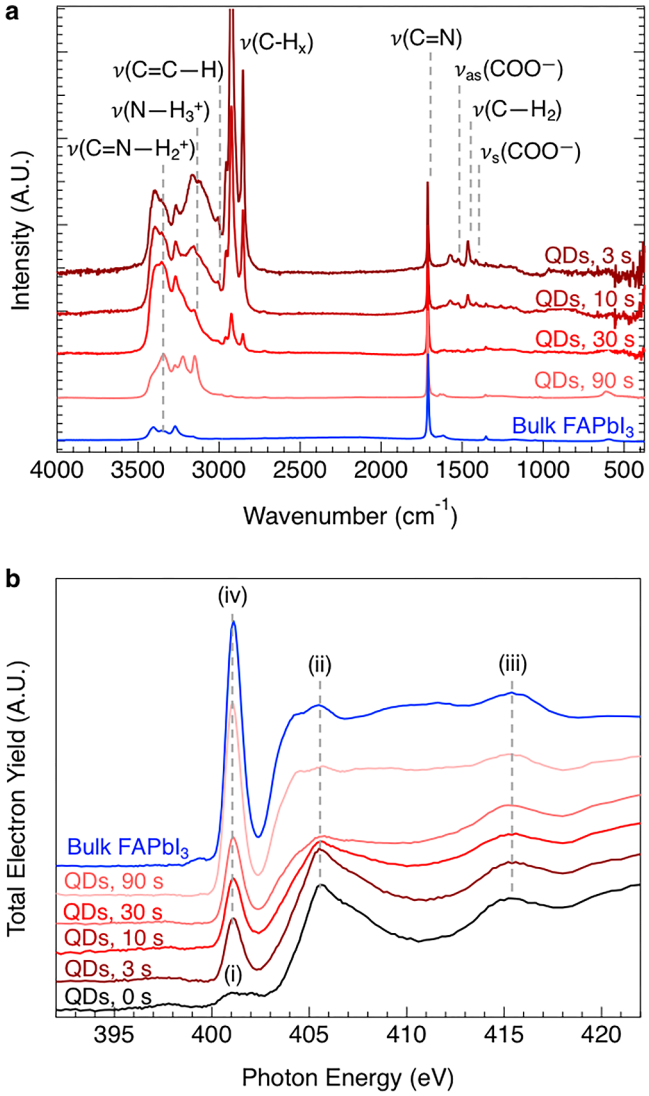

Figure 3. (a) FTIR and (b) N K-edge XAS spectra of $CsPbI_3$ QD films treated with MeOAc and then with solutions of saturated FAI in EtOAc for between 3 and 90 s (shades of red). The treated QD films are compared to a bulk $FAPbI_3$ film (blue). FTIR spectra are normalized to the ν(C=N) resonance and offset for clarity.

FTIR is used to investigate FAI treatment chemistry (Figure 3a). $CsPbI_3$ QD films are first built up into films using multiple cycles of spin-coating and MeAOc treatment described above in processing environments between 14% and 24% RH. The MeOAc process is followed by treating with FAI for varying amounts of time by immersing the film in a saturated solution of FAI in EtOAc. We find the degree of ligand exchange varies greatly with time. After 3 s (dark red spectrum, Figure 3a), there are notable changes already to the FTIR spectrum: (1) The presence of formamidinium is observed by the emergence of ν(C=N) = 1710 cm^{-1} and ν(C=N−H_2^+) = 3460 cm^{-1}. (2) Carboxylate peaks are reduced in relative intensity, suggesting that FAI is displacing cations of oleylammonium or cesium (Cs^+) as well as anions (An^-), including oleate, acetate, and, most likely, iodide (Scheme 1c). Ion-pair exchange becomes clearer at longer soak times. After 10 and 30 s (lighter red spectra, Figure 3) the resonances associated with the oleylammonium (ν(N−H_3^+), ν(C−H_x), ν(C=C−H), and ν(C−H_2)) and carboxylate (ν_s(COO^-) and ν_{as}(COO^-))

DOI: 10.1021/jacs.8b04984
J. Am. Chem. Soc. 2018, 140, 10504−10513

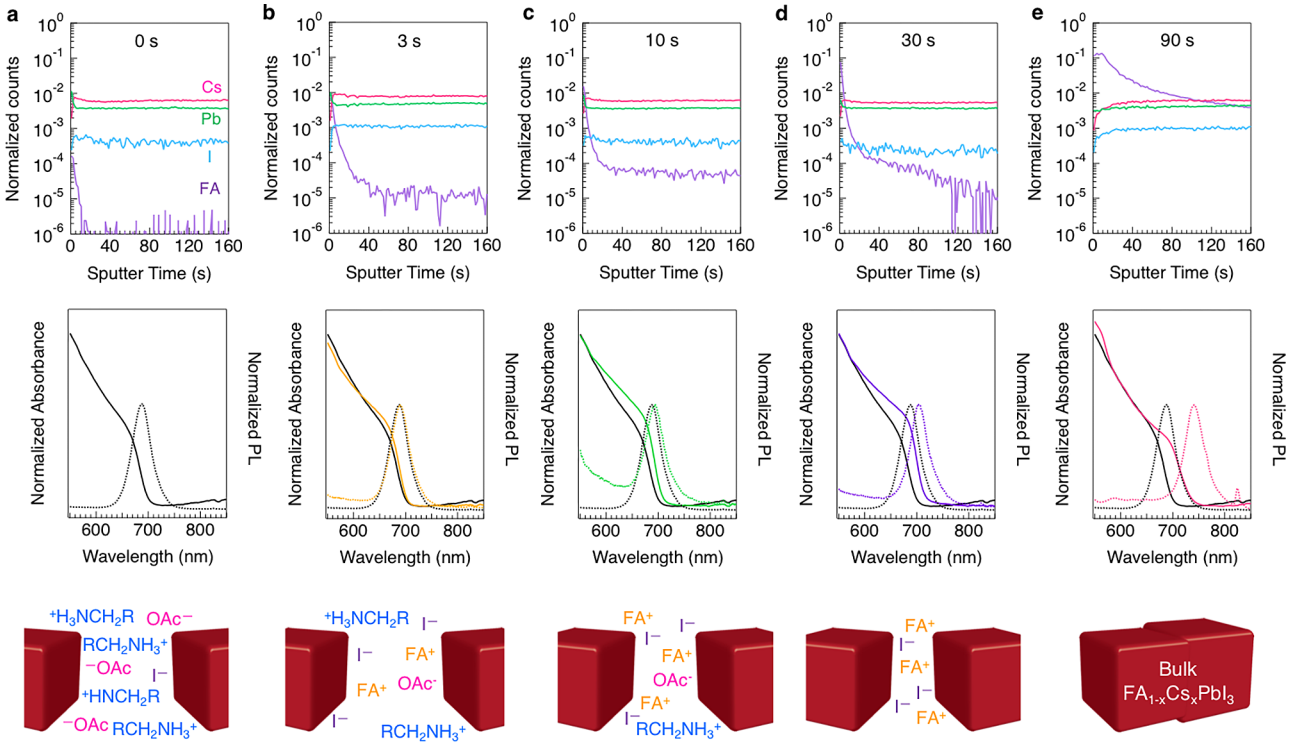

Figure 4. (a) Film composition determined by TOF-SIMs (top) of $CsPbI_3$ QD films as a function of thickness through the film (sputter time) and absorbance and PL (middle) of films treated with MeOAc (a) and then with solutions of FAI in EtOAc for 3 s (b), 10 s (c), 30 s (d), and 90 s (e), and a cartoon of surface composition (bottom). Absorption and PL of the MeOAc-treated film (black) is reproduced in all plots for comparison purposes.

decrease in relative intensity compared to the formamidinium peaks. After 90 s (pink spectrum, Figure 3), resonances due to the surface species are below the FTIR detection limit, and the film changes from brown to yellow in appearance due to relaxation from the α-$CsPbI_3$ phase to the δ-$CsPbI_3$ phase. The 90 s spectrum appears nearly identical to a bulk film of $FAPbI_3$ produced from a molecular precursor (blue spectrum, Figure 3),[39] which is an indication that the individual QDs in the QD film have coalesced to produce an FA-alloyed bulk film in the orthorhombic phase. Bulk alloys of $FA_{1-x}Cs_xPbI_3$, where x = 0.3 and 0.7, also resemble the blue spectrum (QDs, 90 s) in Figure 3a, but the ν(C═N) resonance blueshifts with increasing Cs concentration (Figure S7).

We collected X-ray absorption spectroscopy (XAS) data to further verify the cation-exchange mechanism upon treatment of the $CsPbI_3$ QD films with the FAI solution (Figure 3b). The N K-edge absorption spectra of the respective QD films treated for 0, 3, 10, 30, and 90 s along with a bulk $FAPbI_3$ thin film are depicted in Figure 3b. In the XAS spectra of the control $CsPbI_3$ film (0 s, black curve), three main features are labeled in Figure 3b and are attributed as follows: (i) a small contribution of molecular amine (401−402 eV),[40] (ii) a major contribution of ammonium (405.5 eV), and (iii) a Pb component at the Pb N_5 edge (415 eV). The fingerprint spectrum of the ammonium component corresponds to those in spectra acquired for methylammonium lead iodide films in past studies.[41,42] Upon prolonged treatment with FAI, the ammonium peak in the spectra of the QD films decreases. We concomitantly observe the appearance of a distinct peak at 401 eV, which is attributed to the molecular 1s→π^* transition of the imidine moiety in the FAI unit ((iv) in Figure 3b). The relative intensity of this peak is increasing with exposure of the QD film to the FAI in EtOAc solution (i.e., larger net uptake of FAI) while at the same time the extended part of the post-edge region (404−420 eV) is undergoing a gradual change. We conclude FAI treatment is selective to the QD surface before 30 s. After 90 s of FAI treatment, the post-edge region resembles the one recorded for a bulk $FAPbI_3$ film (blue curve), which indicates that the formamidinium in the QD film will assume a local coordination as in bulk $FAPbI_3$. In contrast to this finding, we compared the lead coordination of a $CsPbI_3$ QD thin film after MeOAc treatment, as well as 0 and 10 s exposure to FAI EtOAc by the Pb L_3 edge in a bulk-sensitive hard X-ray absorption spectroscopy experiment.[43] We find that after 10 s of treatment with FAI in EtOAc, the Pb in the QD films is still coordinated as in a Cs rich $FA_xCs_{1-x}PbI_3$ thin film, due to the lack of the characteristic peaks that are expected at 13 040.7 and 13 045.5 eV for a FA-rich bulk phase (Figure S8). XAS data are consistent with the conclusion that initially FAI selectively exchanges with oleylammonium at the QD surface rather than A-site exchange within QD crystal.

We gain more insight into the FAI treatment chemistry and the incorporation of FA into the bulk material using time-of-flight secondary ion mass spectroscopy (TOF-SIMS). Masses that correspond to components of the $CsPbI_3$ QDs—Cs (m/z = 265.81), Pb (m/z = 205.98), I (m/z = 126.91), and FA (m/z = 45.05)—were tracked as a function of depth through QD films treated with FAI for 0, 3, 10, 30, and 90 s (Figure 4a−e, middle panels). Signal due to Cs remains relatively constant for up to 30 s of FAI treatment, which indicates that (1) there is preferential exchange of oleylammonium at the QD surface as observed in the FTIR data (Figure 3), and (2) FA^+ cations are largely not exchanging with Cs^+ in the bulk of the QD crystal—the FAI treatment is surface selective. It is not until

DOI: 10.1021/jacs.8b04984
J. Am. Chem. Soc. 2018, 140, 10504−10513

90 s that a change in the Cs^+ concentration is observed, which correlates to large increase in the FA concentration and when QDs coalesce together to form a bulk film. Interestingly, treatments that last <30 s show the treatment is uniform across the thickness of the film, and the relative concentration of FA increases with longer treatment times. In contrast, there is a concentration gradient at 90 s after the film has transformed into a FA-rich bulk phase.

Exchange of oleylammonium for FA^+ enhanced the electronic coupling in the QD film as indicated by an increase in the mobility.[29] We further demonstrate this coupling by correlating the TOF-SIMS data to ultraviolet−visible absorption and PL spectroscopies (Figure 4, middle panels). At 0 s, the $CsPbI_3$ QD film shows a symmetric PL emission peak centered at 688 nm and absorption onset at 700 nm (Figure 4a, middle). These spectra are included in Figure 4b−e for comparison. After 3 s, the absorption and emission of the QD film look nearly identical to those of the 0 s sample (Figure 4b). After 10s, the PL emission shifts slightly from 688 to 694 nm, which we attribute to overlap of QD wave functions.[44] Stronger coupling is apparent after 30 s, when a 40 meV PL redshift to 704 nm is observed (Figure 4d). When the QDs coalesce into a bulk film at 90 s, a much more dramatic shift is observed, corresponding to the bandgap of the resulting bulk $FA_{1-x}Cs_xI_3$ film. A cartoon that summarizes the effect of FAI treatment time on the chemistry and inter-QD spacing is illustrated at the bottom of Figure 4.

The $J-V$ scans of photovoltaic devices show characteristics that corroborate insights into treatment time gained from TOF-SIMS. When the FAI treatment is omitted (0 s, Figure 5) the J_{SC} is suppressed due to incomplete removal of the long chain organic ligands that impede charge transport in the QD array. When the FAI treatment is included, the J_{SC} improves from 6.3 to 14.1 mA/cm^2 (3 s), and then to 15.2 and 15.4 mA/cm^2 (10 and 30 s, respectively). This is confirmed in the external quantum efficiency (EQE) spectra (Figure 5b) where the 0 s treatment has <30% response across the entire spectrum, while the EQE of FAI-treated devices reach >80% and are indistinguishable, within error. The 3 s treatment removes the majority of the oleylammonium ligands, but increasing to a 10 s treatment time removes virtually all the remaining electronically insulating ligands. The longer, 30 s treatment time results in a decreased V_{OC} due to the internal cation exchange that begins after the surface ligand exchange is complete. $FAPbI_3$ has a lower bandgap than $CsPbI_3$, so the alloyed material has a lower bandgap than pure $CsPbI_3$, and likely more energetic disorder, thus reducing the V_{OC} in the device. The stabilized power output is also closest to the maximum power point of the reverse scan for the 10 s treatment, indicative of less hysteresis in the device. Therefore, the 10 s treatment time results in the complete removal of long-chain organic ligands without the detrimental effects of cation-exchange in the core of the QD. It is unclear how shorter ligands will impact the thermal stability of PV devices. This is currently being studied.

CONCLUSION

The highly ionic nature of the MHP QD surface make it a new frontier in QD surface chemistry. Previous work has shown surface manipulation is critical in producing high-efficiency QDSCs and near-unity PLQY QD emitters. Here we develop a molecular picture of the chemistry that enables such promising technologies. Notably, we found controlling the amount of adventitious water was paramount for producing high-efficiency

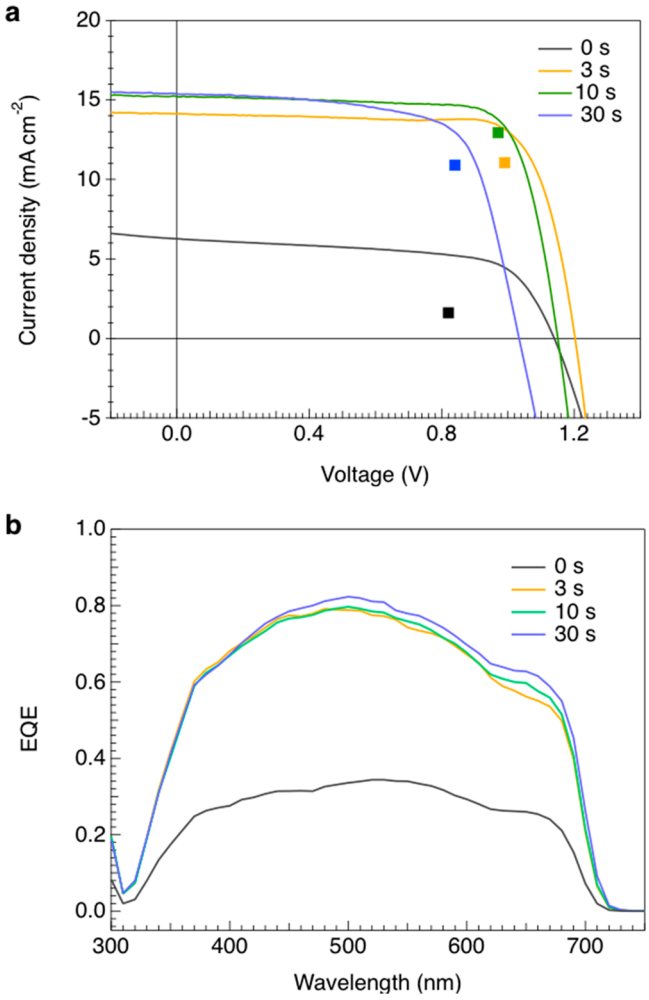

Figure 5. (a) Current density−voltage with stabilized power output shown as square markers and (b) EQE curves for PV devices with $CsPbI_3$ QD absorber layers treated with MeOAc and then with solutions of FAI in EtOAc for times between 3 and 30 s.

QDSCs since water is needed to hydrolyze MeOAc in the process of exchanging native oleate ligands for shorter acetate molecules. QDs were coupled into high-quality optoelectronic films following treatment with solutions of FAI. Ion pairs, including oleylammonium, were exchanged from the QD surface as a function of time, eventually leading to incorporation of FA into the bulk material. We determined the ideal processing window for this treatment, as QDs will couple together more strongly at treatment times ≤30 s but coalesce into bulk film at times >30 s. MeOAc and FAI treatments represent targeted strategies for exchanging electronic−insulating ligands that are native from the QD synthesis. The work represents a detailed chemical understanding in a complex new material with implications for advanced optoelectronic applications and can serve as a guide for researchers aiming to develop novel ligand chemistries for MHP QDs.

EXPERIMENTAL METHODS

Chemicals. All chemicals were purchased from Sigma-Aldrich and used without further purification unless otherwise noted: oleic acid (OA, technical grade 90%), oleylamine (OAm, technical grade 70%), 1-octadecene (ODE, technical grade 90%), toluene (anhydrous, 99.8%), hexane (reagent grade ≥95%), octane (anhydrous, ≥99%), 1-butanol (anhydrous, 99.8%), methyl acetate (MeOAc, anhydrous

DOI: 10.1021/jacs.8b04984
J. Am. Chem. Soc. 2018, 140, 10504−10513

99.5%), ethyl acetate (EtOAc, anhydrous, 99.8%), cesium carbonate (Cs_2CO_3, 99.9%), lead(II) iodide (PbI_2 99.9985%, Alfa Aesar), lead(II) nitrate ($Pb(NO_3)_2$, 99.999%), formamidinium iodide (FAI, Dyesol), ethanol (EtOH, 200 proof, ≥99.5%), titanium diisopropoxide bis(acetylacetonate) (TAA, 75 wt% in isopropanol), 2,2′,7,7′-tetrakis(*N*,*N*-di-*p*-methoxyphenylamine)-9,9′-spirobifluorene (spiro-OMeTAD, Lumtec, ≥99.5%), chlorobenzene (anhydrous, 99.8%), 4-*tert*-butylpyridine (tBP, 96%), bis(trifluoromethane)sulfonimide lithium salt (Li-TFSI), and acetonitrile (anhydrous, 99.8%).

Preparation of Cs-Oleate Precursor for QD Synthesis. In a 100 mL three-necked round-bottom flask, 0.407 g of Cs_2CO_3, 20 mL of ODE, and 1.25 mL of OA were degassed at 100 °C for 20 min. Afterward, the flask was purged with N_2 gas, and the temperature was increased to 150 °C. The reaction was considered complete when the solution was clear, indicating that the Cs_2CO_3 reacted with the OA. The completed Cs-oleate precursor (0.125 M) was stored under N_2 until it was needed for QD synthesis.

Synthesis and Purification of $CsPbI_3$ QDs. $CsPbI_3$ QDs were synthesized using procedures similar to past reports.[3] First, 0.75 g of PbI_2 and 25 mL of ODE were degassed in a 100 mL three-necked round-bottom flask at 110 °C for 20 min. Next, 3.75 mL of OA and 3.75 mL of OAm were mixed, preheated to 130 °C, and injected into the flask. The OA/OAm addition allowed for full dissolution of the PbI_2. Once the PbI_2 was fully dissolved, the flask was purged with N_2 gas, and the temperature was increased to 185 °C. Once the desired temperature was reached, 3 mL of the Cs-oleate precursor was quickly injected into the flask. The reaction was quenched in an ice bath after ∼5 s.

The resultant QDs were purified by mixing each 15 mL of the QD liquor with 35 mL of MeOAc and centrifuging for 5 min at 7500 rpm. The supernatant was discarded, and the QD pellet was redissolved in 5 mL of hexane. Next, ∼5 mL of MeOAc was added to the QDs, and the solution was immediately centrifuged for a second time at 7500 rpm for 5 min. The resultant QD pellet was dissolved in ∼15 mL of hexane and stored at 4 °C for 24 h. This allowed for precipitation of excess Cs-oleate and Pb-oleate from the QD solution. Before use, the QDs were centrifuged at 7500 rpm to remove excess precipitates.

NMR Spectroscopy. ^{1}H NMR spectra were acquired on a 400 MHz Bruker Avance at 25 °C using standard pulse sequences, with 2 s acquisition and 10 s delay between pulses (32 scans per spectrum). Samples were prepared by dissolving centrifuged $CsPbI_3$ nanocrystals in benzene-d_6 at a concentration of ∼20 mg/mL.

$CsPbI_3$ Film Fabrication. $CsPbI_3$ QD films were fabricated using previously reported methods,[16,17] with the exception being controlled humidity environments during the first ligand-exchange step. Saturated solutions of $Pb(NO_3)_2$ in MeOAc and FAI in EtOAc were prepared by adding 20 mg of salt into 20 mL of solvent and sonicating for 10 min. Excess salt was removed by centrifugation at 3500 rpm for 5 min. To prepare the QD film, concentrated $CsPbI_3$ QD solutions (∼75 mg/mL) were spin-cast onto a TiO_2 surface at 1000 rpm for 20 s, followed by 2000 rpm for 5 s. The resulting films were dipped into the $Pb(NO_3)_2$ solution for ∼3 s, followed by rinsing with neat MeOAc for ∼3 s. This process was repeated three times to produce a thick QD film (200−300 nm). During the ligand exchange with the $Pb(NO_3)_2$ solution, the ambient relative humidity (RH) was varied from 0 to 40% RH in a climate-controlled glovebox. Once a thick QD film was deposited, ambient humidity was reduced to 0% RH, and the films were post-treated with saturated solutions of FAI in EtOAc.[17] The films were dipped into the FAI solution for 10 s, followed by rinsing with neat MeOAc.

FTIR Spectroscopy. FTIR was performed in diffuse reflectance mode using a Bruker Alpha FTIR spectrometer inside the argon atmosphere glovebox. Spectra were collected by averaging between 24 and 128 scans at 2 cm^{-1} resolution. Samples were prepared the same way as described in the $CsPbI_3$ film fabrication but on a gold-coated silicon wafer. Spectra of neat OA and OAm liquids were collected in attenuated total reflectance mode using the same spectrometer.

Device Fabrication. TiO_2 was deposited onto pre-patterned FTO-coated glass substrates (Thin Film Devices Inc.) by spin-casting a 0.15 M TAA solution in 1-butanol onto the substrates by the following procedure: 700 rpm for 10 s, 1000 rpm for 10 s, and 2000 rpm for 30 s.[45] The resulting film was annealed at 500 °C for 30 min to form dense TiO_2 films of approximately 20−40 nm thickness. The TiO_2 surface was cleaned with UV-ozone for 15 min prior to the perovskite QD film deposition. A spiro-OMeTAD hole-transport layer was spin-cast at 5000 rpm from a solution consisting of 72 mg of spiro-OMeTAD, 1 mL of chlorobenzene, 28.8 μL of tBP, and 17.5 μL of Li-TFSI solution (520 mg/mL Li-TFSI in acetonitrile). A 15 nm layer of MoO_3 was thermally evaporated at a rate of 0.1−0.5 Å/s, and then a 200 nm Al layer was thermally evaporated at a rate of 0.5−2.0 Å/s to complete the devices.

Photoemission Spectroscopy. PES measurements were performed on a Kratos NOVA spectrometer calibrated to the Fermi edge and core-level positions of sputter-cleaned metal (Au, Ag, Cu, Mo) surfaces. Ultraviolet photoemission spectra were acquired from the He I (21.22 eV) excitation line at a nominal experimental resolution below 150 meV. X-ray photoemission spectra were taken using monochromated Al Kα radiation (1486.7 eV) at a resolution of 400 meV.

X-ray Absorption Spectroscopy. All XAS measurements were carried out at the Stanford Synchrotron Radiation Lightsource (SSRL). Soft X-ray XAS measurements were performed on beamline 8-2 using linearly polarized X-rays at normal and grazing incidence with respect to the surface normal. Spectra were collected in total electron yield (TEY) mode via the drain current and normalized by photon flux on a freshly evaporated gold grid. Hard X-ray XAS measurements were made with the high-resolution spectrometer at SSRL beamline 6-2.[46] The incident energy was selected along the vicinity of the Pb L_3-edge using a double-crystal liquid-nitrogen-cooled Si(311) monochromator. The incident X-ray flux at the target position was estimated to be ∼3×10^{12} photons/s, and the beam size full width at half-maximum was measured to be ∼120×400 μm^2 (vertical by horizontal). The Rowland circle spectrometer (R = 1 m) used seven Si(880) crystals with 100 mm diameter aligned to the maximum of the Pb Lβ5 emission line (13014.3 eV). The energy resolution was measured to be ∼1.5 eV.

TOF-SIMS Characterization. Secondary ion mass spectrometry (SIMS) is a powerful analytical technique for determining elemental and isotopic distributions in solids, as well as the structure and composition of organic materials.[47] An ION-TOF TOF-SIMS V time-of-flight SIMS (TOF-SIMS) spectrometer was utilized for depth profiling. Analysis was completed utilizing a three-lens, 30 keV BiMn primary ion gun: the Bi_3^+ primary-ion beam (operated in bunched mode; 10 ns pulse width, pulsed analysis current 0.8 pA) was scanned over a 50 micron by 50 micron area. Depth profiling was accomplished with a 0.6 keV oxygen ion (3 nA sputter current) sputter beam, rastering over a 200 micron by 200 micron area. All spectra during profiling were collected at or below a primary ion dose density of 1×10^{12} ions cm^{-2} to remain at the static-SIMS limit. The data are plotted with the intensity for each signal at each data point normalized to the total ion counts measured at that data point, which diminishes artifacts from a changing ion yield across different samples and potential beam damage.

■ ASSOCIATED CONTENT

Supporting Information

The Supporting Information is available free of charge on the ACS Publications website at DOI: 10.1021/jacs.8b04984.

Additional XPS, UPS, XAS, and FTIR spectra and photographs of photovoltaic devices (PDF)

■ AUTHOR INFORMATION

Corresponding Authors

*lance.wheeler@nrel.gov

*joey.luther@nrel.gov

ORCID

Lance M. Wheeler: 0000-0002-1685-8242

Jeffrey A. Christians: 0000-0002-6792-9741

DOI: 10.1021/jacs.8b04984
J. Am. Chem. Soc. 2018, 140, 10504−10513

Steven P. Harvey: 0000-0001-6120-7062
Lih Y. Lin: 0000-0001-9748-5478
Joseph M. Luther: 0000-0002-4054-8244

Notes

The authors declare no competing financial interest.

■ ACKNOWLEDGMENTS

This work was authored in part by Alliance for Sustainable Energy, LLC, the manager and operator of the National Renewable Energy Laboratory (NREL) for the U.S. Department of Energy (DOE), under Contract No. DE-AC36-08GO28308. J.M.L. and A.R.M. acknowledge support by the Center for Advanced Solar Photophysics, an Energy Frontier Research Center funded by the U.S. Department of Energy, Office of Science, Office of Basic Energy Sciences. L.M.W. and N.C.A. acknowledge support from the Laboratory Directed Research and Development (LDRD) program and NREL. S.P.H. and J.J.B. acknowledge support from the DOE Solar Energy Technology Office (SETO) Hybrid Perovskite Solar Cell Program. E.M.S. and L.Y.L. were supported by a National Aeronautics and Space Administration (NASA) Space Technology Research Fellowship. J.A.C. was supported by the DOE Energy Efficiency and Renewable Energy (EERE) Postdoctoral Research Award under the EERE SETO, administered by the Oak Ridge Institute for Science and Education (ORISE) for the DOE under DOE contract no. DE-SC00014664. M.S. acknowledges the DOE, Office of Science, Office of Workforce Development for Teachers and Scientists (WDTS) under the Science Undergraduate Laboratory Internships (SULI) program at NREL. P.S. acknowledges the French Agence Nationale de la Recherche for funding under contract no. ANR-17-MPGA-0012. D.N., D.S., and T.K. acknowledge the U.S. Department of Energy, Office of Science, Office of Basic Energy Sciences. This research was partly carried out at the Stanford Synchrotron Radiation Lightsource, a National User Facility operated by Stanford University on behalf of the U.S. Department of Energy, Office of Basic Energy Sciences, under Contract No. DE-AC02-76SF00515.

■ REFERENCES

(1) Zhang, W.; Eperon, G. E.; Snaith, H. J. *Nat. Energy* **2016**, *1* (6), 16048.
(2) Protesescu, L.; Yakunin, S.; Bodnarchuk, M. I.; Krieg, F.; Caputo, R.; Hendon, C. H.; Yang, R. X.; Walsh, A.; Kovalenko, M. V. *Nano Lett.* **2015**, *15* (6), 3692.
(3) Akkerman, Q. A.; D'Innocenzo, V.; Accornero, S.; Scarpellini, A.; petrozza, A.; Prato, M.; Manna, L. *J. Am. Chem. Soc.* **2015**, *137* (32), 10276.
(4) Protesescu, L.; Yakunin, S.; Kumar, S.; Bär, J.; Bertolotti, F.; Masciocchi, N.; Guagliardi, A.; Grotevent, M.; Shorubalko, I.; Bodnarchuk, M. I.; Shih, C.-J.; Kovalenko, M. V. *ACS Nano* **2017**, *11* (3), 3119.
(5) De Roo, J.; Ibáñez, M.; Geiregat, P.; Nedelcu, G.; Walravens, W.; Maes, J.; Martins, J. C.; Van Driessche, I.; Kovalenko, M. V.; Hens, Z. *ACS Nano* **2016**, *10*, 2071.
(6) Wheeler, L. M.; Anderson, N. C.; Palomaki, P. K. B.; Blackburn, J. L.; Johnson, J. C.; Neale, N. R. *Chem. Mater.* **2015**, *27* (19), 6869.
(7) Hanrahan, M. P.; Fought, E. L.; Windus, T. L.; Wheeler, L. M.; Anderson, N. C.; Neale, N. R.; Rossini, A. J. *Chem. Mater.* **2017**, *29* (24), 10339.
(8) Wheeler, L. M.; Levij, L. M.; Kortshagen, U. R. *J. Phys. Chem. Lett.* **2013**, *4* (20), 3392.
(9) Wheeler, L. M.; Nichols, A. W.; Chernomordik, B. D.; Anderson, N. C.; Beard, M. C.; Neale, N. R. *Nano Lett.* **2016**, *16* (3), 1949.
(10) Owen, J. S.; Park, J.; Trudeau, P.-E.; Alivisatos, A. P. *J. Am. Chem. Soc.* **2008**, *130* (37), 12279.
(11) Chen, P. E.; Anderson, N. C.; Norman, Z. M.; Owen, J. S. *J. Am. Chem. Soc.* **2017**, *139* (8), 3227.
(12) Nag, A.; Kovalenko, M. V.; Lee, J.-S.; Liu, W.; Spokoyny, B.; Talapin, D. V. *J. Am. Chem. Soc.* **2011**, *133* (27), 10612.
(13) Kovalenko, M. V.; Kaufmann, E.; Pachinger, D.; Roither, J.; Huber, M.; Stangl, J.; Hesser, G.; Schäffler, F.; Heiss, W. *J. Am. Chem. Soc.* **2006**, *128* (11), 3516.
(14) Anderson, N. C.; Hendricks, M. P.; Choi, J. J.; Owen, J. S. *J. Am. Chem. Soc.* **2013**, *135* (49), 18536.
(15) Luther, J. M.; Law, M.; Song, Q.; Perkins, C. L.; Beard, M. C.; Nozik, A. J. *ACS Nano* **2008**, *2* (2), 271.
(16) Marshall, A. R.; Young, M. R.; Nozik, A. J.; Beard, M. C.; Luther, J. M. *J. Phys. Chem. Lett.* **2015**, *6* (15), 2892.
(17) Lin, Q.; Yun, H. J.; Liu, W.; Song, H.-J.; Makarov, N. S.; Isaienko, O.; Nakotte, T.; Chen, G.; Luo, H.; Klimov, V. I.; Pietryga, J. M. *J. Am. Chem. Soc.* **2017**, *139* (19), 6644.
(18) Sim, K. M.; Swarnkar, A.; Nag, A.; Chung, D. S. *Laser Photonics Rev.* **2018**, *12* (1), 1700209.
(19) Li, J.; Xu, L.; Wang, T.; Song, J.; Chen, J.; Xue, J.; Dong, Y.; Cai, B.; Shan, Q.; Han, B.; Zeng, H. *Adv. Mater.* **2017**, *29* (5), 1603885.
(20) Ravi, V. K.; Santra, P. K.; Joshi, N.; Chugh, J.; Singh, S. K.; Rensmo, H.; Ghosh, P.; Nag, A. *J. Phys. Chem. Lett.* **2017**, *8*, 4988.
(21) Akkerman, Q. A.; Rainò, G.; Kovalenko, M. V.; Manna, L. *Nat. Mater.* **2018**, *17* (5), 394.
(22) Pan, J.; Quan, L. N.; Zhao, Y.; Peng, W.; Murali, B.; Sarmah, S. P.; Yuan, M.; Sinatra, L.; Alyami, N. M.; Liu, J.; Yassitepe, E.; Yang, Z.; Voznyy, O.; Comin, R.; Hedhili, M. N.; Mohammed, O. F.; Lu, Z. H.; Kim, D. H.; Sargent, E. H.; Bakr, O. M. *Adv. Mater.* **2016**, *28* (39), 8718.
(23) Pan, J.; Sarmah, S. P.; Murali, B.; Dursun, I.; Peng, W.; Parida, M. R.; Liu, J.; Sinatra, L.; Alyami, N.; Zhao, C.; Alarousu, E.; Ng, T. K.; Ooi, B. S.; Bakr, O. M.; Mohammed, O. F. *J. Phys. Chem. Lett.* **2015**, *6* (24), 5027.
(24) Swarnkar, A.; Marshall, A. R.; Sanehira, E. M.; Chernomordik, B. D.; Moore, D. T.; Christians, J. A.; Chakrabarti, T.; Luther, J. M. *Science* **2016**, *354* (6308), 92.
(25) Luther, J. M.; Law, M.; Beard, M. C.; Song, Q.; Reese, M. O.; Ellingson, R. J.; Nozik, A. J. *Nano Lett.* **2008**, *8* (10), 3488.
(26) Ip, A. H.; Thon, S. M.; Hoogland, S.; Voznyy, O.; Zhitomirsky, D.; Debnath, R.; Levina, L.; Rollny, L. R.; Carey, G. H.; Fischer, A.; Kemp, K. W.; Kramer, I. J.; Ning, Z.; Labelle, A. J.; Chou, K. W.; Amassian, A.; Sargent, E. H. *Nat. Nanotechnol.* **2012**, *7*, 577.
(27) Chernomordik, B. D.; Marshall, A. R.; Pach, G. F.; Luther, J. M.; Beard, M. C. *Chem. Mater.* **2017**, *29* (1), 189.
(28) Kim, S.; Marshall, A. R.; Kroupa, D. M.; Miller, E. M.; Luther, J. M.; Jeong, S.; Beard, M. C. *ACS Nano* **2015**, *9* (8), 8157.
(29) Sanehira, E. M.; Marshall, A. R.; Christians, J. A.; Harvey, S. P.; Ciesielski, P. N.; Wheeler, L. M.; Schulz, P.; Lin, L. Y.; Beard, M. C.; Luther, J. M. *Sci. Adv.* **2017**, *3* (10), eaao4204.
(30) Wheeler, L. M.; Anderson, N. C.; Bliss, T. S.; Hautzinger, M. P.; Neale, N. R. *J. Phys. Chem. C* **2018**, *122*, 14029.
(31) Tackett, J. E. *Appl. Spectrosc.* **1989**, *43*, 483.
(32) Kroupa, D. M.; Voros, M.; Brawand, N. P.; McNichols, B. W.; Miller, E. M.; Gu, J.; Nozik, A. J.; Sellinger, A.; Galli, G.; Beard, M. C. *Nat. Commun.* **2017**, *8*, 15257.
(33) Dou, B.; Wheeler, L. M.; Christians, J. A.; Moore, D. T.; Harvey, S. P.; Berry, J. J.; Barnes, F. S.; Shaheen, S. E.; van Hest, M. F. A. M. *ACS Energy Lett.* **2018**, *3*, 979.
(34) Noel, N. K.; Congiu, M.; Ramadan, A. J.; Fearn, S.; McMeekin, D. P.; Patel, J. B.; Johnston, M. B.; Wenger, B.; Snaith, H. J. *Joule* **2017**, *1* (2), 328.
(35) Ikari, A.; Hatate, Y.; Futai, M.; Kurokawa, Y. *J. Chem. Eng. Data* **1985**, *30* (2), 163.

DOI: 10.1021/jacs.8b04984
J. Am. Chem. Soc. 2018, 140, 10504−10513

(36) Xue, J.; Zhang, Z.; Zheng, F.; Xu, Q.; Xu, J.; Zou, G.; Li, L.; Zhu, J.-J. *Anal. Chem.* **2017**, *89* (16), 8212.
(37) Bowen, C. R.; Kim, H. A.; Weaver, P. M.; Dunn, S. *Energy Environ. Sci.* **2014**, *7*, 25.
(38) Chiba, T.; Hoshi, K.; Pu, Y.-J.; Takeda, Y.; Hayashi, Y.; Ohisa, S.; Kawata, S.; Kido, J. *ACS Appl. Mater. Interfaces* **2017**, *9* (21), 18054.
(39) Li, Z.; Yang, M.; Park, J.-S.; Wei, S.-H.; Berry, J. J.; Zhu, K. *Chem. Mater.* **2016**, *28* (1), 284.
(40) Gordon, M. L.; Cooper, G.; Morin, C.; Araki, T.; Turci, C. C.; Kaznatcheev, K.; Hitchcock, A. P. *J. Phys. Chem. A* **2003**, *107* (32), 6144.
(41) McLeod, J. A.; Wu, Z.; Shen, P.; Sun, B.; Liu, L. *J. Phys. Chem. Lett.* **2014**, *5* (16), 2863.
(42) Pérez-del-Rey, D.; Forgács, D.; Hutter, E. M.; Savenije, T. J.; Nordlund, D.; Schulz, P.; Berry, J. J.; Sessolo, M.; Bolink, H. J. *Adv. Mater.* **2016**, *28* (44), 9839.
(43) Drisdell, W. S.; Leppert, L.; Sutter-Fella, C. M.; Liang, Y.; Li, Y.; Ngo, Q. P.; Wan, L. F.; Gul, S.; Kroll, T.; Sokaras, D.; Javey, A.; Yano, J.; Neaton, J. B.; Toma, F. M.; Prendergast, D.; Sharp, I. D. *ACS Energy Lett.* **2017**, *2* (5), 1183.
(44) Liu, Y.; Gibbs, M.; Puthussery, J.; Gaik, S.; Ihly, R.; Hillhouse, H. W.; Law, M. *Nano Lett.* **2010**, *10* (5), 1960.
(45) Ahn, N.; Son, D.-Y.; Jang, I.-H.; Kang, S. M.; Choi, M.; Park, N.-G. *J. Am. Chem. Soc.* **2015**, *137* (27), 8696.
(46) Sokaras, D.; Weng, T.-C.; Nordlund, D.; Alonso-Mori, R.; Velikov, P.; Wenger, D.; Garachtchenko, A.; George, M.; Borzenets, V.; Johnson, B.; Rabedeau, T.; Bergmann, U. *Rev. Sci. Instrum.* **2013**, *84* (5), 053102.
(47) Stevie, F. A. *Secondary Ion Mass Spectrometry: Applications for Depth Profiling and Surface Characterization*; Momentum Press, 2015.

DOI: 10.1021/jacs.8b04984
J. Am. Chem. Soc. 2018, 140, 10504−10513